

Time-reversal invariant topological moiré flat band: A platform for the fractional quantum spin Hall effect

Yi-Ming Wu,¹ Daniel Shaffer,² Zhengzhi Wu,³ and Luiz H. Santos²

¹Stanford Institute for Theoretical Physics, Stanford University, Stanford, California 94305, USA

²Department of Physics, Emory University, 400 Dowman Drive, Atlanta, Georgia 30322, USA

³Institute for Advanced Study, Tsinghua University, Beijing 100084, China



(Received 6 October 2023; revised 11 February 2024; accepted 20 February 2024; published xxxxxxxxxx)

Motivated by recent observation of the quantum spin Hall effect in monolayer germanene and twisted bilayer transition-metal dichalcogenides (TMDs), we study the topological phases of moiré twisted bilayers with time-reversal symmetry and spin s_z conservation. By using a continuum model description, which can be applied to both germanene and TMD bilayers, we show that at small twist angles the emergent moiré flat bands can be topologically nontrivial due to inversion symmetry breaking. Each of these flat bands admits a lowest-Landau-level description for each spin projection in the chiral limit and at magic twist angle. This allows for the construction of a many-body Laughlin state with time-reversal symmetry, which can be stabilized by a short-range pseudopotential, and therefore serves as an ideal platform for realizing the so-far elusive fractional quantum spin Hall effect with emergent spin-1/2 U(1) symmetry.

DOI: [10.1103/PhysRevB.00.005100](https://doi.org/10.1103/PhysRevB.00.005100)

I. INTRODUCTION

Since the discovery of superconducting and correlated insulating phases in magic-angle twisted bilayer graphene (TBG) [1–12], the moiré engineering of 2D van der Waals materials, such as graphene and transition metal dichalcogenides (TMDs) [13–23], in a host of bilayer and multilayer heterostructures [24–32], has attracted enormous research attention. Moiré platforms are ideal hubs to forge the interplay between strongly correlated effects and topological phases, giving rise to rich phenomena including superconductivity [1,6–8], strange metal behavior [33–35], magnetic quantum anomalous Hall effect in TBG [9,36,37] and more recently, long-sought after fractional Chern insulators (FCI) [38–40] first observed in twisted bilayer MoTe₂ [41–44].

The discovery of FCIs in TMD heterostructures highlights the importance of moiré flat bands [45–53] in the service of electron fractionalization without a magnetic field. In particular, moiré flat bands in the chiral limit [48] share properties akin to lowest Landau level (LLL) wavefunctions, shedding light on the stability of time-reversal broken topological states through local interactions [54–59]. Conversely, a burning question arises: Can moiré flat bands support *time-reversal symmetric (TRS) fractional* topological order? While TRS \mathbb{Z}_2 flat bands have been theoretically proposed in twisted bilayer TMDs [60–64], and experimental signatures of the quantum spin Hall (QSH) effect [65–71] have been noted in twisted bilayer TMD [72–74], prospects for fractional QSH effect in moiré systems remain *terra incognita*.

In this paper, we propose a mechanism to realize TRS topological \mathbb{Z}_2 moiré flat bands and establish them as potential platforms to achieve fractional quantum spin Hall effect [67,75–77] through electron interactions in moiré heterostructures. Our point of departure is a continuum model of small-angle twisted bilayer heterostructures, which can be applied to bilayer TMD or the paradigmatic Kane-Mele

(KM) model [65]. The KM model was recently realized in a mono-elemental honeycomb material—germanene [78]. Two layers of KM model are generally expected to be topologically trivial given the instability of the double pairs of helical edge modes [65]. However, our analysis of the small-angle twisted bilayer KM model identifies topological phase transitions, which can be tuned by the twist angle, interlayer coupling and sublattice potential. The resulting quasiflat moiré bands are characterized by a TRS \mathbb{Z}_2 topological invariant signaling a new pair of helical edge states. Remarkably, in the chiral limit where the AA interlayer coupling vanishes, the wavefunction for each flat band behave as a Kramer’s pair of time-reversal invariant lowest-level Landau (LLL) wavefunctions containing both holomorphic and antiholomorphic coordinates related by time reversal. As such, our paper identifies key aspects enabling TRS electron fractionalization in twisted moiré bilayers. In particular, we propose classes of many-body wavefunctions hosting fractional QSH, which is stabilized by certain short-range interactions. This paper thus puts forth a promising route to explore fractional QSH in \mathbb{Z}_2 flat bands of moiré heterostructures. Our consideration may also apply to cold atom platforms for which moiré engineering has also been made possible recently [79].

II. MODEL

A low-energy description of both monolayer TMD and germanene with spin $s = \uparrow, \downarrow \equiv \pm 1$ and valley $\tau = \pm 1$ rotated by an angle θ is given by (setting $\hbar = 1$)

$$h_{s\tau}(\theta, \mathbf{k}) = \tau |\mathbf{k}| v_F \begin{pmatrix} 0 & e^{-i\tau(\theta_k - \theta)} \\ e^{i\tau(\theta_k - \theta)} & 0 \end{pmatrix} + \delta \sigma_z + \lambda s \tau \gamma. \quad (1)$$

Here θ_k is the angle between \mathbf{k} and some reference axis. δ in the case of TMD denotes the sublattice potential

83 difference while in germanene it can arise from coupling to
 84 substrate [80]. λ is the spin-orbit coupling (SOC) strength, and
 85 $\gamma = \text{diag}(\gamma_1, \gamma_2)$. For TMDs [81] we have $\gamma = (1 - \sigma_z)/2$,
 86 while for germanene $\gamma = \sigma_z$, as in the Kane-Mele model [65].
 87 Equation (1) preserves time-reversal (\mathcal{T}) symmetry, and an
 88 emergent U(1) symmetry for the spin s_z component. When
 89 two layers of TMD or germanene described by Eq. (1) are
 90 stacked and twisted by a small angle, the moiré pattern devel-
 91 ops as is shown in Fig. 1(a). The emergent moiré periodicity
 92 gives rise to much smaller moiré Brillouin zone shown in
 93 Fig. 1(b). Following [45], the continuum model for both
 94 twisted bilayer TMD and germanene systems can thus be
 95 described in a uniform way. For spin s and valley τ , the
 96 Hamiltonian written explicitly in the two layer space is

$$H_{s\tau} = \begin{pmatrix} h_{s\tau}(\frac{\theta}{2}, \nabla) & T_{\tau}(\mathbf{r}) \\ T_{\tau}^{\dagger}(\mathbf{r}) & h_{s\tau}(-\frac{\theta}{2}, \nabla) \end{pmatrix}, \quad (2)$$

97 where $h_{s\tau}(\theta/2, \nabla) = -i\tau v_F R[\sigma \cdot \nabla]R^{-1} + \delta\sigma_z + \lambda s\tau\gamma$ is the
 98 real-space representation of Eq. (1) (with $R = e^{-i\frac{\theta}{4}\sigma_z}$),
 99 and the local interlayer coupling $T(\mathbf{r})$ captures the moiré
 100 superlattice. The Hamiltonian acts on a spinor $\psi_{s\tau} =$
 101 $(\psi_{A1}, \psi_{B1}, \psi_{A2}, \psi_{B2})^T$, where A, B and $1, 2$ are sublattice and
 102 layer indices, respectively. As in TBG, the interlayer coupling
 103 can be approximated by $T_{\pm}(\mathbf{r}) = \sum_{n=1}^3 T_n e^{-i\mathbf{q}_n \cdot \mathbf{r}}$ where $\mathbf{q}_1 =$
 104 $k_{\theta}(0, -1)$, $\mathbf{q}_2 = k_{\theta}(\sqrt{3}/2, 1/2)$ and $\mathbf{q}_3 = k_{\theta}(-\sqrt{3}/2, 1/2)$
 105 with $k_{\theta} = 2k_D \sin(\theta/2)$ being the moiré Brillouin zone length
 106 scale and k_D is the distance between Γ point and K point. Note
 107 that for the other valley $T_{-}(\mathbf{r}) = T_{+}^*(\mathbf{r})$. The three coefficients
 108 T_n are $T_{n+1} = w_{AA}I + w'_{AA}\sigma_z + w_{AB}(\sigma_x \cos \frac{2n\pi}{3} + \sigma_y \sin \frac{2n\pi}{3})$,
 109 with w_{AA} (w'_{AA}) and w_{AB} the interlayer tunneling strength in
 110 AA- and AB-stacked areas respectively; w'_{AA} vanishes for
 111 germanene but remains nonzero for TMD.

112 \mathbb{Z}_2 flat bands. Taking twisted bilayer germanene as our
 113 example, the corresponding moiré band structure is shown in
 114 Fig. 1(c), which was obtained by setting $v_F = 5.6 \times 10^5$ m/s,
 115 and $\lambda = 24$ meV [78,82]. Note that v_F is around 70% of that
 116 in graphene. Assuming the interlayer coupling is also around
 117 70% of that in TBG, we approximately take $w_{AB} = 80$ meV
 118 and set $r = w_{AA}/w_{AB}$ as a variable. The two bands marked in
 119 red are the moiré flat bands, separated by a gap due to $\lambda \neq 0$.
 120 The first magic angle at which the moiré bandwidth gets mini-
 121 mized is determined by the condition $\alpha := w_{AB}/(v_F k_{\theta}) \approx$
 122 0.586 [48]. Furthermore, for a given $s\tau$ configuration, the flat
 123 bands have nonzero Chern numbers given by $C_{s,\tau} = \pm \text{sgn}(s)$,
 124 where “+” is for the upper bands and “-” is for the lower
 125 bands. This gives rise to nontrivial topology with TRS, which
 126 is characterized by the \mathbb{Z}_2 topological invariant [69,83]

$$\nu_{\pm} = \frac{C_{\uparrow,\pm} - C_{\downarrow,\mp}}{2} \text{mod} 2. \quad (3)$$

127 Thus the upper moiré band has $\nu_{\pm} = 1$ while the lower moiré
 128 band has $\nu_{\pm} = -1$. The topological phase can be tuned by θ ,
 129 w_{AB} , and w_{AA} , as shown in Fig. 1(d). We also confirmed that at
 130 even larger θ (not shown) the system becomes trivial as well,
 131 consistent with the \mathbb{Z}_2 classification of two layer KM model.

132 The band structure for twisted bilayer TMD are similar
 133 to those shown in Fig. 1(c), except that δ and λ are much
 134 larger than those in germanene, and w'_{AA} can be nonzero due
 135 to the difference between valence and conduction bands. The

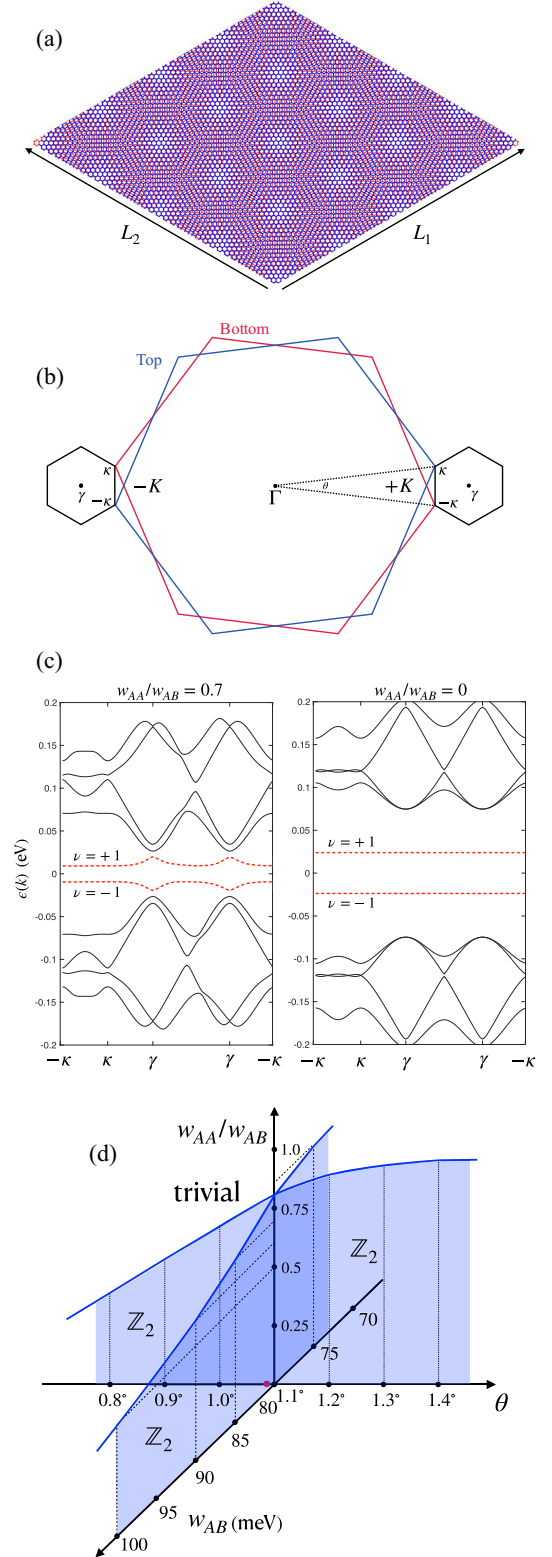


FIG. 1. (a) Moiré pattern with system size given by L_1 and L_2 . (b) Moiré Brillouin zone at $\pm K$ valleys. The definition of $\pm\kappa$ is chosen in such a way that κ at $+K$ is related to $-\kappa$ at $-K$ valley by time reversal. (c) Moiré band structure for $+K$ valley at the first magic angle $\theta = 1.09^\circ$, obtained by choosing $w_{AB} = 80$ meV and $\delta = 0$. (d) Three-dimensional phase diagram with $\delta \neq 0$. The \mathbb{Z}_2 phase appears as a bulk region, of which the two orthogonal cross sections are shown in blue. For a fixed w_{AA} and w_{AB} , tuning θ can result in a topological phase transition from a \mathbb{Z}_2 band to a trivial

136 large band gap resulting from δ in TMD has a remarkable
137 consequence of large sublattice polarization, which we will
138 explain in the following.

139 III. TOPOLOGICAL FLATBAND

140 The Hamiltonian in Eq. (2) has an emergent chiral sym-
141 metry when w_{AA} and w'_{AA} vanish. In this limit and at
142 the magic twist angle, there are two exactly flat bands
143 for each spin and valley [see Fig. 1(c)] whose energy
144 is determined solely by λ and δ . To see this, we can
145 first rotate the basis to $\tilde{\chi}_{s\tau} = \text{diag}(e^{i\theta\sigma_z/4}, e^{-i\theta\sigma_z/4})\psi_{s\tau} \equiv$
146 $(\chi_{A1}, \chi_{B1}, \chi_{A2}, \chi_{B2})^T$, and then rewrite the Hamiltonian in a
147 new basis $\chi_{s\tau} = (\chi_{A1}, \chi_{A2}, \chi_{B1}, \chi_{B2})^T \equiv (\chi_A, \chi_B)^T$. The re-
148 sulting eigenvalue equation becomes

$$\begin{pmatrix} \lambda s\tau\gamma_1 + \delta & D_\tau^*(-\mathbf{r}) \\ D_\tau(\mathbf{r}) & \lambda s\tau\gamma_2 - \delta \end{pmatrix} \begin{pmatrix} \chi_A \\ \chi_B \end{pmatrix} = \varepsilon \begin{pmatrix} \chi_A \\ \chi_B \end{pmatrix}, \quad (4)$$

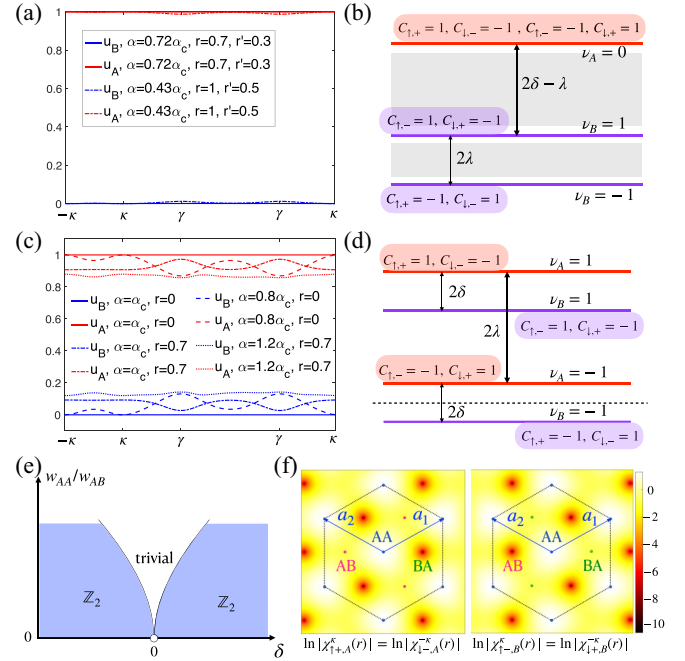
149 where

$$D_+(\mathbf{r}) = \begin{pmatrix} -2iv_F\partial_z & U_+(\mathbf{r}) \\ U_+(-\mathbf{r}) & -2iv_F\partial_z \end{pmatrix}, \quad D_-(\mathbf{r}) = D_+^*(\mathbf{r}), \quad (5)$$

150 $U_+(\mathbf{r}) = w_{AB}(e^{-iq_1\cdot\mathbf{r}} + e^{i\phi}e^{-iq_2\cdot\mathbf{r}} + e^{-i\phi}e^{-iq_3\cdot\mathbf{r}})$ and $\partial_z \equiv \frac{\partial}{\partial z} =$
151 $(\partial_x + i\partial_y)/2$. Equation (4) has an apparent solution in a fully
152 sublattice-polarized form with either $\chi_A = 0$ or $\chi_B = 0$ for
153 all \mathbf{r} . If we assume $\chi_B = 0$, then Eq. (4) is solved by $\varepsilon =$
154 $\lambda s\tau\gamma_1 + \delta$ and $D_\tau(\mathbf{r})\chi_A = 0$. The latter condition is in fact
155 identical to the zero-energy flat-band equation for chiral TBG
156 [47]. The other set of solution with the opposite sublattice
157 polarization is found by assuming $\chi_A = 0$, which has the
158 energy $\varepsilon = \lambda s\tau\gamma_2 - \delta$.

159 The sublattice polarization is not just a fine tuning effect
160 of the chiral limit and a similar effect has been discussed in
161 lattice models [84–86]. In Figs. 2(a) and 2(c), we show the
162 sublattice weight for the top-most flat band for twisted bilayer
163 TMD and germanene respectively [87]. For TMD bilayers, the
164 sublattice polarization is always almost maximized for a wide
165 range of parameters, while for germanene bilayers, it is maxi-
166 mized only when the system is near the chiral limit and magic
167 angle ($\alpha \rightarrow \alpha_c$ and $r \rightarrow 0$). In Figs. 2(b) and 2(d) we show the
168 Chern numbers for the four flat bands, which help us to further
169 identify the \mathbb{Z}_2 flat bands according to Eq. (3). For TMD
170 bilayers, since we neglected the SOC in the conduction band,
171 there are only two \mathbb{Z}_2 flat bands with B-sublattice polarization,
172 which are separated from many other bands due to large λ
173 [gray area in Fig. 2(b)]. In contrast, the germanene bilayers
174 can host four energetically close \mathbb{Z}_2 flat bands. If the Fermi
175 level is located in the middle of the lower two bands, then
176 tuning δ results in a topological phase transition as indicated
177 in Fig. 2(e), where in the chiral limit the trivial regime shrinks
178 to a point at $\delta = 0$.

179 The wavefunction for these chiral flat bands can be ob-
180 tained in a similar fashion as for TBG flat bands [47]. For
181 simplicity, we consider the top-most band. For $\tau = +1$, the
182 equation $D_+(\mathbf{r})\chi_A(\mathbf{r}) = 0$ has a C_3 -rotation symmetry pro-
183 tected solution at the moiré Brillouin corner $\pm\kappa$, which we
184 denote as $\chi_{\uparrow\pm}^{\pm\kappa}$ ($\pm\kappa$ are related by C_3 rotation so below we use
185 $\chi_{\uparrow\pm}^{\pm\kappa}$ only). Because $D_+(\mathbf{r})$ contains only the antiholomorphic
186 derivative ∂_z , the general solution is $\chi_{\uparrow\pm}^{\pm\kappa}(\mathbf{r}) = f_k(z)\chi_{\uparrow\pm}^{\pm\kappa}(\mathbf{r})$
187 where $\partial_z f_k(z) = 0$ and $z \equiv x + iy$ is the complex coordinate.



188 FIG. 2. [(a),(b)] Sublattice weight and moiré flat bands for
189 twisted bilayer TMD. In (a) we choose the upper flat band with
190 $s = +$ and $\tau = +$ and α is reduced by increasing θ . Due to a large
191 δ and λ in TMD, the sublattice polarization is almost maximized for
192 different α , r , and r' . The A(B)-sublattice polarized flat bands are
193 shown in red(purple), and gray regions denote other dispersive moiré
194 bands. [(c),(d)] Sublattice weight and moiré flat band for twisted
195 bilayer germanene. We again choose $s = +$ and $\tau = +$ for (c). Here
196 the since δ and λ are much smaller than those in TMD, all the
197 four resulting \mathbb{Z}_2 flat bands are energetically close to each other.
198 (e) Schematics of the phase diagram when the Fermi level is at the
199 dashed line shown in (d). (f) Plots of the wavefunction amplitude at
200 the moiré κ point in log scale. The zeros are located at $\pm(a_1 - a_2)/3$
201 depending on s and τ .

202 $f_k(z)$ must have simple poles to preserve the moiré lattice
203 translation symmetry, but remarkably each component of
204 $\chi_{\uparrow\pm}^{\pm\kappa}(\mathbf{r})$ has zeros at some particular \mathbf{r}_0 right at the magic
205 twist angle. Therefore, one can locate the poles of $f_k(z)$ at
206 these \mathbf{r}_0 to make $\chi_{\uparrow\pm, \mathbf{k}}^{\pm\kappa}(\mathbf{r})$ a bounded function. In Fig. 2(f)
207 we plot $|\chi_{\uparrow\pm}^{\pm\kappa}(\mathbf{r})|$ on a logarithmic scale. The zeros are located
208 at either AB- or BA-stacking points, depending on s , τ , and
209 sublattice. For A-sublattice polarized bands, $\mathbf{r}_0 = (a_1 - a_2)/3$
210 when measured from the AA center.

211 The total wavefunction can be more conveniently ex-
212 pressed when the spatial origin is shifted to \mathbf{r}_0 , so that

$$\chi_{\uparrow\pm, \mathbf{k}}^{\pm\kappa}(\mathbf{r}) = F_{\uparrow\pm}(\mathbf{r})N(\mathbf{k}) \left[e^{i\frac{k_x z}{2}} \sigma \left(z + i\frac{S}{2\pi}k \right) \right] \quad (6)$$

213 where

$$F_{\uparrow\pm}(\mathbf{r}) = \frac{\chi_{\uparrow\pm}^{\pm\kappa}(\mathbf{r} + \mathbf{r}_0) e^{-\frac{\pi a_1^* z^2}{2S a_1}}}{\vartheta_1\left(\frac{z}{a_1}, \frac{a_2}{a_1}\right)}, \quad N(\mathbf{k}) = \frac{\pi \vartheta'(0, \frac{a_2}{a_1})}{a_1} e^{\frac{S a_1^* k^2}{8\pi a_1}}. \quad (7)$$

214 Here $a_j \equiv a_{j_x} + ia_{j_y}$ for $j = 1, 2$ and $k \equiv k_x + ik_y$ are the
215 complex number representations of vectors, and $S = |a_1 \times$
216

a_2] is the area of the moiré unit cell. $\vartheta_1(u, \eta)$ is one of the Jacobi theta functions [88], which has the double-periodic properties $\vartheta_1(u + n, \eta) = (-1)^n \vartheta_1(u, \eta)$ and $\vartheta_1(u + n\eta, \eta) = (-1)^n e^{-i\pi(2nu+n^2\eta)} \vartheta_1(u, \eta)$ for $n \in \mathbb{Z}$, and vanishes at $u = n + m\eta$ for $n, m \in \mathbb{Z}$ such that $1/\vartheta_1(u, \eta)$ has simple poles at these positions. As a result, $F(\mathbf{r})$ becomes regular. The universal part, [...] in the above equation, contains a modified Weierstrass sigma function [89], which has zeros on the moiré lattice sites, and is related to ϑ_1 via $\sigma(z) = \frac{a_1}{\pi} \exp\left(\frac{\pi a_1^2 z^2}{2S a_1}\right) \vartheta_1\left(\frac{z}{a_1}, \eta\right) / \vartheta_1'(0, \eta)$ (see also Appendix A for details). The time-reversal counterpart $\chi_{\downarrow-,k}(\mathbf{r})$ is constructed in the same manner.

We note that the zeros of $\chi_{\uparrow+}^k$ and $\chi_{\downarrow-}^k$ coincide in space [see Fig. 2(f)], and they can be made complex conjugate to each other. Furthermore, the operator $D_-(\mathbf{r})$ contains only holomorphic derivatives, indicating the wavefunction for $\tau = -1$ valley contains only antiholomorphic functions. Clearly this construction is equivalent to taking the complex conjugate of $\chi_{\uparrow+,k}$, and we thus have

$$\chi_{\downarrow-,k}(\mathbf{r}) = F_{\downarrow-}(\mathbf{r}) N^*(\mathbf{k}) \left[e^{-i\frac{kz^*}{2}} \sigma\left(z^* - i\frac{S}{2\pi} k^*\right) \right] \quad (8)$$

with $F_{\downarrow-}(\mathbf{r}) = F_{\uparrow+}^*(\mathbf{r})$. Using the quasiperiodic properties of the theta function, it is straightforward to check that both of these wavefunctions indeed satisfy Bloch's theorem [90].

Equations (6) and (8) are quite similar to the LLL wavefunction on a torus in the symmetric gauge [91], which is obtained by taking $F(\mathbf{r}) = e^{-|z|^2/4}$ and $N(\mathbf{k}) = e^{-|k|^2/4}$ (setting magnetic length $l_B = 1$ for simplicity), and $\sigma(z)$ is defined for an arbitrary lattice as long as the unit-cell area is $S = 2\pi$ (one flux quantum per unit cell). In fact, for any 2D ideal flat band with Chern number $\mathcal{C} = 1$, its wavefunction can be written in the form of Eq. (6) with some properly chosen $F(\mathbf{r})$ and $N(\mathbf{k})$ [92,93] (also see Appendix B for details). The flat band being ideal means that the cell-periodic part, defined as $u_{s\tau,k}(\mathbf{r}) = e^{i\mathbf{r}\cdot\mathbf{k}} \chi_{s\tau,k}(\mathbf{r})$ is (anti)holomorphic in k for spin up (down). As a key consequence, the quantum geometric tensor $\eta_{\alpha\beta}(\mathbf{k}) := \langle D_\alpha u_k | D_\beta u_k \rangle$ has vanishing determinant at every \mathbf{k} ; here $D_\alpha := \partial_{k_\alpha} - iA_\alpha$ with $A_\alpha = i \langle u_k | \partial_{k_\alpha} u_k \rangle$ the Berry connection. This in turn implies that the Fubini-Study metric $g_{ab}(\mathbf{k})$, the real part of $\eta(\mathbf{k})$, is related to the Berry curvature $\mathbf{\Omega}(\mathbf{k}) = \nabla_{\mathbf{k}} \times \mathbf{A}$ via $g_{\alpha\beta}(\mathbf{k}) = \frac{1}{2} |\mathbf{\Omega}(\mathbf{k})| \delta_{\alpha\beta}$. It is known that these properties make the flat band an ideal system to mimic the Girvin-MacDonald-Platzman (GMP) algebra [94] for the LLL in a strong magnetic field: $[\rho_{q_1}, \rho_{q_2}] = i\mathbf{\Omega} \mathbf{q}_1 \times \mathbf{q}_2 \rho_{\mathbf{q}_1 + \mathbf{q}_2}$ with ρ_q being the density operator projected to the flat band, if we identify the average Berry curvature $\Omega = \frac{1}{S_{\text{BZ}}} \int d\mathbf{k} \mathbf{\Omega}(\mathbf{k})$ as the square of the magnetic length l_B^2 [95–97]. It is this similarity that makes it possible to obtain quantum (spin) Hall effect in the full or partially filled moiré flat bands.

IV. MANY-BODY WAVEFUNCTIONS FOR FQSH

Since Ω plays the same role as l_B^2 in the GMP algebra, we can identify each moiré unit cell as the magnetic unit cell, which hosts a single magnetic flux. For a parallelogram system with the widths $L_1 = N_1 a_1$ and $L_2 = N_2 a_2$ as shown in Fig. 1(a), the general twisted periodic boundary condition for each particle on the many-body wavefunction implies

$\Psi(\{z_i\} | z_j = L_{1,2}) = e^{i\phi_{1,2}} \Psi(\{z_i\} | z_j = 0)$, where $\phi_{1,2}$ are not necessarily zero. Following the logic of Ref. [54,91], we have for spin-up fermions (see Appendix A for details)

$$\Psi_{\uparrow,m}(\{z_j\}) = e^{iKZ} \prod_{j=1}^{N_e} F_{\uparrow+}(\mathbf{r}_j) \prod_{v=1}^m \sigma_L(Z - iZ_v) \times \prod_{i<j} [\sigma_L(z_i - z_j)]^m, \quad (9)$$

where we have assumed there are N_e spin-up fermions so that the filling fraction is $1/m = N_e/N_s$. Note that we need to keep m an odd integer in order to maintain fermionic properties. Here $Z = \sum_j z_j$ and the values of K and $Z_0 := \sum_v Z_v$ are chosen to satisfy

$$e^{iKL_{1,2}} = (-1)^{N_s + N_{1,2}} e^{i\frac{\pi L_{1,2}^2 Z_0}{N_s S} + i\phi_{1,2}}. \quad (10)$$

The sigma function with subscript ‘‘L’’ is defined similarly to the previous discussion, but with the unit cell enlarged to the whole sample spanned by L_1 and L_2 instead of a_1 and a_2 . Since the sigma function vanishes as $\sigma_L(z) \sim z$ when $z \rightarrow 0$, this wavefunction scales as $(z_i - z_j)^m$ whenever there are two particles approaching each other, so it can be stabilized by some pseudopotential similar to that of Haldane. The difference from Haldane's pseudopotential is that the ideal flat-band pseudopotential not only depends on the relative angular momentum between two particles, but also on their center-of-mass (COM), so that the general form of the interactions can be written as $V(\mathbf{r}_1, \mathbf{r}_2) = \sum_{M,m} v_{M,m} \hat{F}_{M,m}$ where $\hat{F}_{M,m}$ is the projector [92]. This can be traced back to the fact that the LLL wavefunction obeys the magnetic translation group [98] while the ideal flat-band wavefunction in our case does not. One simple realization that stabilize the wavefunction in Eq. (9) is to consider sufficiently short range (Hubbard-like) interactions, for which the COM gets frozen, and the pseudopotential can be modeled by $V(\mathbf{r}) = \sum_{m'=0}^{m'-1} v_{m'} (\nabla^2)^{m'} \sum_i \delta(\mathbf{r} - \mathbf{R}_i)$ where \mathbf{R}_i denote all lattice sites and all $m' > 0$ should be odd. For the spin-down fermions, the construction is exactly the same,

$$\Psi_{\downarrow,m'}(\{\bar{w}_j\}) = e^{-i\bar{Q}\bar{W}} \prod_{j=1}^{N'_e} F_{\downarrow-}(\mathbf{r}_j) \prod_{v=1}^{m'} \sigma_L(\bar{W} - i\bar{W}_v) \times \prod_{i<j} [\sigma_L(\bar{w}_i - \bar{w}_j)]^{m'} \quad (11)$$

with $\bar{W} = \sum_j \bar{w}_j$, and \bar{Q} and $\bar{W}_0 := \sum_v \bar{W}_v$ satisfying conditions similar to Eq. (10).

Upon combining the two spin components (9) and (11), we identify

$$\Psi_{\text{FQSH}}(\{z_j, w_j\}) = \Psi_{\uparrow,m}(\{z_j\}) \Psi_{\downarrow,m'}(\{\bar{w}_j\}) \quad (12)$$

as a candidate wavefunction describing a FQSH state with spin-filling fraction $\nu_{\text{spin}} = \frac{1}{m}$, which hosts conserved spin current and fractional electronic excitations [67,75–77]. In short samples compared with the electron mean free path, the presence of a helical edge state may be revealed by the low-temperature (compared to the many-body gap) quantization of the longitudinal conductance $G = 2e^2/h$ [99], expected to

297 persist for an interacting Luttinger liquid edge [100]. Fur-
 298 thermore, charge fractionalization could be sensed via shot
 299 noise measurements [101,102], providing two complementary
 300 experimental signatures of time-reversal symmetric fraction-
 301 alization.

302 Remarkably, the ideal flat-band condition [54,92] ensures
 303 that (12) is the ground state of a local time-reversal symmet-
 304 ric Haldane pseudopotential interaction, which establishes a
 305 microscopic mechanism for time-reversal invariant fractional
 306 topological order in moiré flat-band systems. The many-body
 307 wavefunction (12) can be generalized by multiplication by
 308 terms $\sim \prod_{r<s} (z_r - \bar{w}_s)^n$, which represent correlations be-
 309 tween opposite spins [67,77]. Achieving such FQSH states
 310 would require different local interactions, a question that mer-
 311 its further investigation.

312 V. CONCLUSIONS AND DISCUSSION

313 We have shown that twisted bilayer 2D materials with spin-
 314 orbit coupling (TMD and germanene) can give rise to ideal flat
 315 bands with TRS at magic twist angle and in the chiral limit,
 316 serving as an ideal platform for realizing FQSH effect. There
 317 are, however, two obstacles that can potentially destroy the
 318 FQSH state. The first one is the competition with other sym-
 319 metry breaking phases, including charge density wave due to
 320 long range interactions [103] and ferromagnetism [104]. The
 321 true ground state depends on the details of the interactions,
 322 so given that moiré systems have much higher tunability of
 323 interactions compared to other platforms, we expect that the
 324 FQSH state considered here is indeed in a physically accessi-
 325 ble regime. The second obstacle is that a finite w_{AA} spoils the
 326 ideal flat-band condition and renders the Berry curvature more
 327 inhomogeneous in \mathbf{k} space. Comparing energies of different
 328 competing states in this case, e.g., using exact diagonalization
 329 and DMRG, is an interesting question, which we leave for a
 330 future study. We also note that if intervalley coherence that
 331 spoils s_z conservation is included, a different type of FQSH
 332 without s_z conservation can also be realized.

333 *Note added.* Recently, we noticed that the experimental
 334 breakthrough on observing FQSH has been announced, based
 335 on the twisted bilayer MoTe₂ system [105].

336 ACKNOWLEDGMENTS

337 We thank Fengcheng Wu, Trithep Devakul, Ben
 338 Feldman, Qiong Ma, Sri Raghu, and Steven Kivelson for
 339 useful discussions. This research was supported by the
 340 Gordon and Betty Moore Foundation's EPiQS Initiative
 341 through GBMF8686 (Y.-M.W.), and by the U.S. Department
 342 of Energy, Office of Science, Basic Energy Sciences, under
 343 Award DE-SC0023327 (D.S. and L.H.S.).

344 APPENDIX A: LLL WAVEFUNCTION ON A TORUS AND 345 THE CONSTRUCTION OF LAUGHLIN WAVEFUNCTION

346 The LLL wavefunction on a torus was first studied in
 347 Ref. [91], where the theta function was used to account for
 348 the double-periodicity nature of the wavefunction. There the
 349 theta function is periodic in terms of the boundaries L_1 and L_2 ,
 350 which necessarily involves a product of many theta functions.

Alternatively, one can define the problem on a lattice, and
 the unit cell is chosen arbitrarily but must enclose an area of
 $2\pi l_B^2$ through which a unit flux passes. The introducing of a
 lattice makes it easy to compare with real lattice systems with
 a flat Chern band. Below we discuss both of these pictures
 separately.

1. LLL without lattice

a. Single-particle wavefunction

Here we closely follow the logic of Ref. [91]. The sin-
 gle particle LLL wavefunction in Landau gauge $\mathbf{A}(\mathbf{r}) =$
 $(-yB, 0, 0)$ can be written as

$$\psi(x, y) = e^{-y^2/2} f(z). \quad (\text{A1})$$

Here we have set $l_B^2 = 1$, and $f(z)$ is a holomorphic function
 defined on the whole plane. Due to the presence of the expo-
 nentially decaying prefactor $e^{-y^2/2}$, $f(z)$ can be unbounded in
 the y direction, so the total wavefunction $\psi(x, y)$ can still be
 normalizable. The magnetic translation operator $t(\mathbf{L})$ acting
 on a wavefunction is (assuming \mathbf{B} is in the z direction)

$$t(\mathbf{L})\psi(\mathbf{r}) \equiv \psi(\mathbf{r} + \mathbf{L}) = e^{i\mathbf{L}\cdot[-i\nabla - e\mathbf{A}(\mathbf{r})] + ie\mathbf{B}\cdot(\mathbf{r}\times\mathbf{L})}\psi(\mathbf{r}). \quad (\text{A2})$$

Suppose we defined the system size as a parallelogram with
 width $|L_1|$ and $|L_2|$ and angle φ between them. Then the
 total flux piercing this sample is given by

$$N_s = \frac{A}{2\pi l_B^2} = \frac{|L_1||L_2|\sin\varphi}{2\pi}. \quad (\text{A3})$$

The twisted boundary condition on the wave function implies,

$$\psi(L_{1,2}) = \psi(0)e^{i\phi_{1,2}}. \quad (\text{A4})$$

Let us further assume L_1 is in the x direction without loss of
 generality. Then we can immediately see

$$f(L_1) = f(0)e^{i\phi_1}. \quad (\text{A5})$$

The boundary condition in L_2 direction also applies to the
 prefactor $e^{-y^2/2}$, so we will have

$$e^{-(L_2)\sin\varphi/2} f(L_2) = f(0)e^{i\phi_2}. \quad (\text{A6})$$

Using the definition of N_s , we can also write the above expres-
 sion as

$$e^{-\pi N_s \frac{|L_2|}{|L_1|} \sin\varphi} f(L_2) = f(0)e^{i\phi_2}. \quad (\text{A7})$$

The solution of the above two boxed equations are given by
 the Jacobi theta function,

$$f(z) = e^{ikz} \prod_{v=1}^{N_s} \vartheta_1\left(\frac{z - z_v}{L_1}, \tilde{\eta}\right), \quad (\text{A8})$$

where $\tilde{\eta} = L_2/L_1$ and the theta function ϑ_1 is defined as

$$\vartheta_1(u, \tilde{\eta}) := -i \sum_{l \in \mathbb{Z}} (-1)^l q^{(l+1/2)^2} e^{i\pi(2l+1)u}, \quad q := e^{i\pi\tilde{\eta}}, \quad (\text{A9})$$

which has the following properties:

$$\begin{aligned} \vartheta_1(u + n, \tilde{\eta}) &= (-1)^n \vartheta_1(u, \tilde{\eta}), \\ \vartheta_1(u + n\tilde{\eta}, \tilde{\eta}) &= (-1)^n e^{-i\pi(2nu+n^2\tilde{\eta})} \vartheta_1(u, \tilde{\eta}), \end{aligned}$$

$$\begin{aligned}
\vartheta_1(-u, \tilde{\eta}) &= -\vartheta_1(u, \tilde{\eta}), \\
\vartheta_1(u, \tilde{\eta}) &= 0 \text{ for } u = n + m\tilde{\eta}, \quad m, n \in \mathbb{Z} \\
\vartheta_1(u, \tilde{\eta}) &\sim u \text{ for } u \rightarrow 0.
\end{aligned} \tag{A10}$$

We now need to choose proper k and z_v in order to satisfy the boxed boundary condition in Eqs. (A5) and (A7). Using the properties of ϑ_1 listed above, and defining $z_0 = \sum_{v=1}^{N_s} z_v$, it is easy to see that k and z_0 satisfy the following equations:

$$\begin{aligned}
e^{ikL_1} &= (-1)^{N_s} e^{i\phi_1}, \\
e^{ikL_2} &= (-1)^{N_s} e^{i(\phi_2 - 2\pi z_0/L_1 + \pi N_s \frac{|L_2|}{|L_1|} \cos \varphi)}.
\end{aligned} \tag{A11}$$

Note that the second equation is slightly different from that in Ref. [91], to which it reduces when $\varphi = \pi/2$, i.e., when the L_1 and L_2 are perpendicular to each other. From Eq. (A11) it is easy to see that, if (k, z_0) is the solution, so is $(k + n_1 2\pi/L_1, z_0 - n_1 L_2 + n_2 L_1)$ with $n_1, n_2 \in \mathbb{Z}$. The number of the linearly independent solutions is equal to the number of zeros of $f(z)$, which is N_s .

b. The Laughlin wavefunction

The construction of the many-body Laughlin wavefunction proceeds as follows. Suppose there are N_e electrons, so the filling factor is given by $N_e/N_s = 1/m$. We will assume $m \geq 3$ is some odd integer. The wavefunction is given by the ansatz,

$$\Psi(\{z_i\}) = F(Z) \prod_{i < j} g(z_i - z_j), \tag{A12}$$

where $F(Z)$ is a function, which depends on the center-of-mass coordinate Z and $g(z_i - z_j)$ is the Jastrow factor, which only depends on the relative coordinate. Recall the usual Laughlin wavefunction is

$$\Psi_{\text{LW}}(\{z_i\}) = e^{-\sum_i |z_i|^2/4} \prod_{i < j} (z_i - z_j)^m, \tag{A13}$$

hence we need

$$g(z_i - z_j) \sim (z_i - z_j)^m \text{ for } z_i \rightarrow z_j. \tag{A14}$$

One possibility is

$$g(z) = \left[\vartheta_1\left(\frac{z}{L_1}, \tilde{\eta}\right) \right]^m, \tag{A15}$$

which leads to the following boundary condition for a generic single particle, say z_1 :

$$\begin{aligned}
g(L_1 - z_j) &= (-1)^m g(-z_j), \\
g(L_2 - z_j) &= (-1)^m e^{-im\pi\left(-2\frac{z_j}{L_1} + \frac{L_2}{L_1}\right)} g(-z_j).
\end{aligned} \tag{A16}$$

Therefore, for the product of $N_e - 1$ particles, we have

$$\begin{aligned}
\prod_j g(L_1 - z_j) &= (-1)^{N_s - m} \prod_j g(-z_j), \\
\prod_j g(L_2 - z_j) &= (-1)^{N_s - m} e^{i2\pi m \frac{Z}{L_1} - i(N_s - m)\pi \frac{L_2}{L_1}} \prod_j g(-z_j).
\end{aligned} \tag{A17}$$

If we require that the total wavefunction satisfies

$$\Psi_{\text{LW}}(\{z_j | z_i = L_{1,2}\}) = \Psi_{\text{LW}}(\{z_j | z_i = 0\}) e^{i\phi_{1,2}} \tag{A18}$$

then the center-of-mass factor $F(Z)$ must satisfy

$$\begin{aligned}
F(Z + L_1) &= F(Z) (-1)^{N_s - m} e^{i\phi_1}, \\
F(Z + L_2) &= F(Z) (-1)^{N_s - m} e^{-i2\pi m \frac{Z}{L_1} + i(N_s - m)\pi \frac{L_2}{L_1}} e^{i\phi_2}.
\end{aligned} \tag{A19}$$

The general solution for $F(Z)$ can be expressed as

$$F(Z) = e^{iKZ} \prod_{v=1}^m \vartheta_1\left(\frac{Z - Z_v}{L_1}, \tilde{\eta}\right). \tag{A20}$$

Likewise, we need to properly choose K and $Z_0 := \sum_v Z_v$ to solve Eq. (A19). This puts constraints on K and Z_0 , namely

$$\begin{aligned}
e^{iKL_1} &= (-1)^{N_s} e^{i\phi_1}, \\
e^{iKL_2} &= (-1)^{N_s} e^{-i2\pi \frac{Z_0}{L_1}} e^{iN_s \pi \tilde{\eta}} e^{i\phi_2}.
\end{aligned} \tag{A21}$$

2. Another choice: LLL wavefunction with a lattice

a. Symmetric gauge

Here it is useful to switch to symmetric gauge where $\mathbf{A} = (-yB/2, xB/2, 0)$, the magnetic translation operator acting on $\psi(\mathbf{r})$ has a simple form (again assuming $eB = l_B^{-2} = 1$)

$$t(\mathbf{L}) = e^{i\mathbf{L} \cdot (-i\nabla) + \frac{i}{2}(\mathbf{r} \times \mathbf{L}) \cdot \hat{z}}. \tag{A22}$$

The wavefunction that simultaneously diagonalize the Hamiltonian and this translation operator can be given by the modified Weierstrass sigma function [89]

$$\sigma(z) = a_1 e^{\frac{\pi a_1^* z^2}{2S a_1}} \frac{\vartheta_1\left(\frac{z}{a_1}, \eta\right)}{\vartheta_1'(0, \eta)}, \tag{A23}$$

where ϑ_1 is the theta function defined above, and ϑ_1' denotes its derivative. S is the area of the unit cell, and in the lattice spanned by a_1 and a_2 we have $S = 2\pi$. Upon translated by a lattice $l = ma_1 + na_2$ with $m, n \in \mathbb{Z}$, it changes as

$$\sigma(z + l) = \xi(l) e^{\frac{\pi i^*}{S}(z+l/2)} \sigma(z), \tag{A24}$$

where $\xi(l) = 1$ if $l/2$ is also on the lattice and $\xi(l) = -1$ otherwise. In particular, if $l = a_j$ with $j = 1, 2$, we have

$$\sigma(z + a_j) = -e^{\frac{a_j^*}{2}(z+a_j/2)} \sigma(z). \tag{A25}$$

Now if we write the wavefunction as

$$\psi_S(x, y) = e^{-|z|^2/4} f_k(z) \tag{A26}$$

then the holomorphic function $f_k(z)$ is given by

$$f_k(z) = \sigma(z + ik) e^{-|k|^2/4 + ik^* z/2}. \tag{A27}$$

An important property of writing the LLL wavefunction using this modified sigma function is that it does not depend on the specific choice of the lattice, i.e., it is modular invariant. One can design an artificial lattice spanned by the lattice vector \mathbf{a}_1 and \mathbf{a}_2 with the unit cell area being 2π ($2\pi l_B^2$ when l_B is not set to unity). Then the system under consideration can be described using two integers N_1 and N_2 , such that $L_1 = N_1 a_1$ and $L_2 = N_2 a_2$, and the total number of fluxes passing through the system is given by $N_s = N_1 N_2$. Under

437 translation $\mathbf{l} = m\mathbf{a}_1 + n\mathbf{a}_2$, this wavefunction transforms as

$$\begin{aligned}\psi_S(\mathbf{r} + \mathbf{l}) &= e^{-|z+l|^2/4} f_k(z+l) \\ &= e^{-\frac{|z+l|^2}{4} - \frac{|l|^2}{4} - \frac{z^*l + l^*z}{4} + i\frac{k^*z + kz^*l}{2}} \sigma(z+l+ik) \\ &= \xi(l) e^{i\frac{k^*l + l^*k}{2} + \frac{l^*z - z^*l}{4}} \psi_S(\mathbf{r}) \\ &= \xi(l) e^{ik \cdot \mathbf{l} + \frac{i}{2}(\mathbf{r} \times \mathbf{l}) \cdot \hat{z}} \psi_S(\mathbf{r}).\end{aligned}\quad (\text{A28})$$

438 Note this wavefunction transforms in a similar but not exactly
439 the same way as a Bloch wavefunction transforms under spa-
440 tial translation. Using this properties, one can explicitly show
441 that

$$t(\mathbf{l}_1)t(\mathbf{l}_2)\psi_S(\mathbf{r}) = t(\mathbf{l}_2)t(\mathbf{l}_1)\psi_S(\mathbf{r})e^{i(\mathbf{l}_1 \times \mathbf{l}_2) \cdot \hat{z}} \quad (\text{A29})$$

442 as it should be. The periodic boundary condition in Eq. (A4)
443 then implies \mathbf{k} must obey

$$\begin{aligned}\mathbf{k} \cdot \mathbf{L}_1 &= 2\pi n_1 + N_1\pi + \phi_1, \\ \mathbf{k} \cdot \mathbf{L}_2 &= 2\pi n_2 + N_2\pi + \phi_2,\end{aligned}\quad (\text{A30})$$

444 with $n_1, n_2 \in \mathbb{Z}$.

445 Using the relation between the sigma function and the
446 theta function it is possible to express the wavefunction only
447 in terms of the theta function. In addition, without loss of
448 generality, we can always choose a_1 to be real. It is then easy
449 to see

$$\psi_S(x, y) = e^{i\frac{k a_1}{a_1} z} a_1 e^{-\frac{|z|^2 - z^2}{4} - \frac{|k|^2 + k^2}{4}} \vartheta_1\left(\frac{z + ik}{a_1}, \omega\right). \quad (\text{A31})$$

450 Note this expression is different from Eq. (A8) in the sense
451 that it contains only one holomorphic theta function. But the
452 number of zeros enclosed by the sample boundary remains the
453 same. It is easy to realize that the function

$$u_k := \psi_S(\mathbf{r}) e^{-ik \cdot \mathbf{r}} \equiv N_k \tilde{u}_k(\mathbf{r}) \quad (\text{A32})$$

454 is a normalized k -holomorphic function $\tilde{u}_k(\mathbf{r})$ times a
455 \mathbf{k} -dependent complex normalization factor N_k (such that
456 $||u_k||^2 = |N_k|^2$). This observation is useful, since the quantum
457 geometric tensor $\eta(\mathbf{k})$, defined as

$$\eta_{ab}(\mathbf{k}) = \frac{\langle \partial_{k_a} u_k | \partial_{k_b} u_k \rangle}{|N_k|^2} - \frac{\langle \partial_{k_a} u_k | u_k \rangle \langle u_k | \partial_{k_b} u_k \rangle}{|N_k|^4} \quad (\text{A33})$$

458 is actually independent of N_k . A simple manipulation shows
459 that when substituting $u_k = N_k \tilde{u}_k$ into this definition, the
460 derivatives of N_k from the first and the second part of
461 Eq. (A33) cancel out, which leads to

$$\eta_{ab}(\mathbf{k}) = \langle \partial_{k_a} \tilde{u}_k | \partial_{k_b} \tilde{u}_k \rangle - \langle \partial_{k_a} \tilde{u}_k | \tilde{u}_k \rangle \langle \tilde{u}_k | \partial_{k_b} \tilde{u}_k \rangle. \quad (\text{A34})$$

462 Therefore, the factor N_k , although depending on \mathbf{k} , does not
463 determine the properties of the ideal flat band.

464 We close by noting that the wavefunction in Landau gauge
465 can be readily obtained by applying the gauge transformation,
466 namely,

$$\begin{aligned}\psi_L(x, y) &= \psi_S(x, y) e^{-ixy/2} \\ &= e^{i\frac{k a_1}{a_1} z} a_1 e^{-\frac{y^2}{2} - \frac{|k|^2 + k^2}{4}} \vartheta_1\left(\frac{z + ik}{a_1}, \omega\right).\end{aligned}\quad (\text{A35})$$

b. The Laughlin wavefunction

467 Using the sigma function, we can write the ansatz for
468 the many-body wavefunction similar to that in Eq. (A12),
469 but since we will be using sigma functions, we write the
470 ansatz as
471

$$\Psi(\{z_i\}) = e^{-\sum_i \frac{|z_i|^2}{4}} F(Z) \prod_{i < j} g(z_i - z_j), \quad (\text{A36})$$

472 where $g(z)$ is now given by

$$g(z) = [\sigma_L(z)]^m \quad (\text{A37})$$

473 and

$$\sigma_L(z) = \frac{L_1}{\pi} e^{\frac{L_1^* z^2}{4N_s L_1}} \vartheta_1\left(\frac{z}{L_1}, \tilde{\eta}\right) / \vartheta'(0, \tilde{\eta}). \quad (\text{A38})$$

474 Similar to Eq. (A25),

$$\sigma_L(z + L_{1,2}) = -e^{\frac{L_{1,2}^* z^2}{2N_s} (z + L_{1,2}/2)} \sigma(z). \quad (\text{A39})$$

475 Clearly $g(z)$ still scales as z^m when $z \rightarrow 0$. Then it is easy to
476 see, similar to Eq. (A17), we now have

$$\begin{aligned}\prod_j g(L_1 - z_j) &= (-1)^{N_s - m} e^{\frac{L_1^* z^2}{4N_s} (N_s - m) - \frac{mL_1^*}{2N_s} Z} \prod_j g(-z_j), \\ \prod_j g(L_2 - z_j) &= (-1)^{N_s - m} e^{\frac{L_2^* z^2}{4N_s} (N_s - m) - \frac{mL_2^*}{2N_s} Z} \prod_j g(-z_j).\end{aligned}\quad (\text{A40})$$

477 Accordingly, the periodic boundary condition on the many-
478 body wave function, when applied to one of the many
479 particles, leads to the following constraints for $F(Z)$:

$$\begin{aligned}\frac{F(Z + L_1)}{F(Z)} &= (-1)^{-N_s + m} e^{\frac{mL_1^*}{2N_s} (Z + \frac{L_1}{2})} e^{i\phi_1}, \\ \frac{F(Z + L_2)}{F(Z)} &= (-1)^{-N_s + m} e^{\frac{mL_2^*}{2N_s} (Z + \frac{L_2}{2})} e^{i\phi_2}.\end{aligned}\quad (\text{A41})$$

480 These equations are solved by assuming the following general
481 form

$$F(Z) = e^{iKZ} \prod_{v=1}^m \sigma_L(Z - iZ_v). \quad (\text{A42})$$

482 Introducing $Z_0 = \sum_{v=1}^m Z_v$, then the parameter K is deter-
483 mined via

$$\begin{aligned}KL_1 &= \frac{L_1^* Z_0}{2N_s} + \pi N_s + \phi_1 + 2n_1\pi, \\ KL_2 &= \frac{L_2^* Z_0}{2N_s} + \pi N_s + \phi_2 + 2n_2\pi,\end{aligned}\quad (\text{A43})$$

484 with $n_1, n_2 \in \mathbb{Z}$. It is also straightforward to see that under
485 translation operation

$$t(\mathbf{L}_1)t(\mathbf{L}_2)\Psi(\{z_i\}) = t(\mathbf{L}_2)t(\mathbf{L}_1)\Psi(\{z_i\})e^{i(\mathbf{L}_1 \times \mathbf{L}_2) \cdot \hat{z}}. \quad (\text{A44})$$

486 **APPENDIX B: THE LAUGHLIN WAVEFUNCTION FOR A**
 487 **GENERIC IDEAL FLAT BAND**

488 From above we see the single particle LLL wavefunction
 489 (in the symmetric gauge) can be conveniently written as

$$\psi(\mathbf{r}) = e^{-\frac{|z|^2}{4}} e^{-\frac{|k|^2}{4}} \left[e^{i\frac{k^*z}{2}} \sigma\left(z + i\frac{S}{2\pi}k\right) \right], \quad (\text{B1})$$

490 where we reintroduced $S = 2\pi l_B^2$ but in our convention $l_B =$
 491 1 it reduces to $S = 2\pi$. It contains three part. The first one
 492 is the factor $e^{-\frac{|z|^2}{4}}$, which depends only on \mathbf{r} and makes sure
 493 the wavefunction decays at large distances. The second term
 494 $e^{-\frac{|k|^2}{4}}$ is a factor, which depends solely on \mathbf{k} . The the last term
 495 inside [...] has the nice property that it becomes a holomorphic
 496 function in k when multiplied by the factor $e^{-ik\cdot\mathbf{r}}$, as

$$\mathbf{k} \cdot \mathbf{r} = \frac{1}{2}(k^*z + z^*k). \quad (\text{B2})$$

497 The many-body Laughlin wavefunction is given by

$$\Psi(\{z_i\}) = e^{iKZ} \left(\prod_{i=1}^{N_e} e^{-\frac{|z_i|^2}{4}} \right) \prod_{v=1}^m \sigma_L(Z - iZ_v) \\ \times \prod_{i<j} [\sigma_L(z_i - z_j)]^m, \quad (\text{B3})$$

498 with K and $Z_0 = \sum_v Z_v$ satisfying Eq. (A43).

499 In fact, as suggested in Ref. [92], any ideal flat-band wave-
 500 function with Chern number $\mathcal{C} = 1$ can be written in a way
 501 similar to Eq. (B1), namely

$$\psi_{\text{IFB}}(\mathbf{r}) = F(\mathbf{r})N(\mathbf{k}) \left[e^{i\frac{k^*z}{2}} \sigma\left(z + i\frac{S}{2\pi}k\right) \right], \quad (\text{B4})$$

502 where $F(\mathbf{r})$ depends on the lattice details, and $N(\mathbf{k})$ is some
 503 normalization factor, which is less important as we already
 504 see in Eqs. (A33) and (A34).

As an example, now let us come back to the magic-angle
 chiral limit flat-band wavefunction for, say $\mathcal{C} = +1$,

$$\chi_{+,k}(\mathbf{r}) = e^{ik\cdot\mathbf{a}_1 \frac{z-z_0}{a_1}} \frac{\vartheta_1\left(\frac{z-z_0}{a_1} - \frac{k}{b_2}, \eta\right)}{\vartheta_1\left(\frac{z-z_0}{a_1}, \eta\right)} \chi_+^k(\mathbf{r}) \\ = e^{ik\cdot\mathbf{a}_1 \frac{z-z_0}{a_1}} \frac{\vartheta_1\left(\frac{z-z_0+i\frac{A}{2\pi}k}{a_1}, \eta\right)}{\vartheta_1\left(\frac{z-z_0}{a_1}, \eta\right)} \chi_+^k(\mathbf{r}). \quad (\text{B5})$$

It is more convenient to work with the wavefunction with ori-
 gin shifted to \mathbf{r}_0 , so we define a new $\tilde{\chi}_{+,k}(\mathbf{r}) = \chi_{+,k}(\mathbf{r} + \mathbf{r}_0)$.
 After some manipulation we rewrite it is as

$$\tilde{\chi}_{+,k}(\mathbf{r}) = \frac{\chi_+^k(\mathbf{r} + \mathbf{r}_0) e^{-\frac{\pi a_1^2 z^2}{2A a_1}} \pi \vartheta'(0, \eta)}{\vartheta_1\left(\frac{z}{a_1}, \eta\right) a_1} e^{\frac{A a_1^2 k^2}{8\pi a_1}} \\ \times \left[e^{i\frac{k^*z}{2}} \sigma\left(z + i\frac{S}{2\pi}k\right) \right]. \quad (\text{B6})$$

From this expression we can easily read off the factors $F(\mathbf{r})$
 and $N(\mathbf{r})$ introduced in Eq. (B4) in this case.

As a directly generalization of Eq. (B3), the many-
 body wavefunction ansatz can be written by modifying
 $F(\mathbf{r})$ accordingly. Therefore, for the magic-angle chiral limit
 flat band, the many-body Laughlin wavefunction ansatz is
 given by

$$\Psi_{\text{IFB}}(\{z_i\}) = e^{iKZ} \left(\prod_{i=1}^{N_e} \frac{\chi_+^k(\mathbf{r}_i + \mathbf{r}_0) e^{-\frac{\pi a_1^2 z_i^2}{2A a_1}}}{\vartheta_1\left(\frac{z_i}{a_1}, \eta\right)} \right) \\ \times \prod_{v=1}^m \sigma_L(Z - iZ_v) \prod_{i<j} [\sigma_L(z_i - z_j)]^m. \quad (\text{B7})$$

Likewise, by using the quasiperiodic properties of σ_L and ϑ_1 ,
 it is easy to see the values of K and $Z_0 = \sum_v Z_v$ must satisfy

$$e^{iKL_1} = (-1)^{N_s+N_1} e^{i\frac{\pi L_1^2 Z_0}{N_s A} + i\phi_1}, \\ e^{iKL_2} = (-1)^{N_s+N_2} e^{i\frac{\pi L_2^2 Z_0}{N_s A} + i\phi_2}, \quad (\text{B8})$$

in order to meet the periodic boundary conditions, which are
 similar to Eq. (A43).

- [1] Y. Cao, V. Fatemi, S. Fang, K. Watanabe, T. Taniguchi, E. Kaxiras, and P. Jarillo-Herrero, Unconventional superconductivity in magic-angle graphene superlattices, *Nature (London)* **556**, 43 (2018).
 [2] Y. Xie, B. Lian, B. Jäck, X. Liu, C.-L. Chiu, K. Watanabe, T. Taniguchi, B. A. Bernevig, and A. Yazdani, Spectroscopic signatures of many-body correlations in magic-angle twisted bilayer graphene, *Nature (London)* **572**, 101 (2019).
 [3] Y. Jiang, X. Lai, K. Watanabe, T. Taniguchi, K. Haule, J. Mao, and E. Y. Andrei, Charge order and broken rotational symmetry in magic-angle twisted bilayer graphene, *Nature (London)* **573**, 91 (2019).

- [4] Y. Choi, J. Kemmer, Y. Peng, A. Thomson, H. Arora, R. Polski, Y. Zhang, H. Ren, J. Alicea, G. Refael *et al.*, Electronic correlations in twisted bilayer graphene near the magic angle, *Nat. Phys.* **15**, 1174 (2019).
 [5] A. Kerelsky, L. J. McGilly, D. M. Kennes, L. Xian, M. Yankowitz, S. Chen, K. Watanabe, T. Taniguchi, J. Hone, C. Dean *et al.*, Maximized electron interactions at the magic angle in twisted bilayer graphene, *Nature (London)* **572**, 95 (2019).
 [6] M. Yankowitz, S. Chen, H. Polshyn, Y. Zhang, K. Watanabe, T. Taniguchi, D. Graf, A. F. Young, and C. R. Dean, Tuning superconductivity in twisted bilayer graphene, *Science* **363**, 1059 (2019).

- [7] X. Lu, P. Stepanov, W. Yang, M. Xie, M. A. Aamir, I. Das, C. Urgell, K. Watanabe, T. Taniguchi, G. Zhang *et al.*, Superconductors, orbital magnets and correlated states in magic-angle bilayer graphene, *Nature (London)* **574**, 653 (2019).
- [8] H. S. Arora, R. Polski, Y. Zhang, A. Thomson, Y. Choi, H. Kim, Z. Lin, I. Z. Wilson, X. Xu, J.-H. Chu *et al.*, Superconductivity in metallic twisted bilayer graphene stabilized by WSe₂, *Nature (London)* **583**, 379 (2020).
- [9] A. L. Sharpe, E. J. Fox, A. W. Barnard, J. Finney, K. Watanabe, T. Taniguchi, M. A. Kastner, and D. Goldhaber-Gordon, Emergent ferromagnetism near three-quarters filling in twisted bilayer graphene, *Science* **365**, 605 (2019).
- [10] S.-Y. Li, Y. Zhang, Y.-N. Ren, J. Liu, X. Dai, and L. He, Experimental evidence for orbital magnetic moments generated by moiré-scale current loops in twisted bilayer graphene, *Phys. Rev. B* **102**, 121406(R) (2020).
- [11] Y. Zhang, Z. Hou, Y.-X. Zhao, Z.-H. Guo, Y.-W. Liu, S.-Y. Li, Y.-N. Ren, Q.-F. Sun, and L. He, Correlation-induced valley splitting and orbital magnetism in a strain-induced zero-energy flatband in twisted bilayer graphene near the magic angle, *Phys. Rev. B* **102**, 081403(R) (2020).
- [12] Y. Saito, J. Ge, L. Rademaker, K. Watanabe, T. Taniguchi, D. A. Abanin, and A. F. Young, Hofstadter subband ferromagnetism and symmetry-broken Chern insulators in twisted bilayer graphene, *Nat. Phys.* **17**, 478 (2021).
- [13] Y. Tang, L. Li, T. Li, Y. Xu, S. Liu, K. Barmak, K. Watanabe, T. Taniguchi, A. H. MacDonald, J. Shan, and K. F. Mak, Simulation of Hubbard model physics in WSe₂/WS₂ moiré superlattices, *Nature (London)* **579**, 353 (2020).
- [14] E. C. Regan, D. Wang, C. Jin, M. I. Bakti Utama, B. Gao, X. Wei, S. Zhao, W. Zhao, Z. Zhang, K. Yumigeta *et al.*, Mott and generalized Wigner crystal states in WSe₂/WS₂ moiré superlattices, *Nature (London)* **579**, 359 (2020).
- [15] Y. Xu, S. Liu, D. A. Rhodes, K. Watanabe, T. Taniguchi, J. Hone, V. Elser, K. F. Mak, and J. Shan, Correlated insulating states at fractional fillings of moiré superlattices, *Nature (London)* **587**, 214 (2020).
- [16] C. Jin, Z. Tao, T. Li, Y. Xu, Y. Tang, J. Zhu, S. Liu, K. Watanabe, T. Taniguchi, J. C. Hone *et al.*, Stripe phases in WSe₂/WS₂ moiré superlattices, *Nat. Mater.* **20**, 940 (2021).
- [17] X. Huang, T. Wang, S. Miao, C. Wang, Z. Li, Z. Lian, T. Taniguchi, K. Watanabe, S. Okamoto, D. Xiao *et al.*, Correlated insulating states at fractional fillings of the WS₂/WSe₂ moiré lattice, *Nat. Phys.* **17**, 715 (2021).
- [18] T. Li, S. Jiang, L. Li, Y. Zhang, K. Kang, J. Zhu, K. Watanabe, T. Taniguchi, D. Chowdhury, L. Fu *et al.*, Continuous Mott transition in semiconductor moiré superlattices, *Nature (London)* **597**, 350 (2021).
- [19] L. Wang, E.-M. Shih, A. Ghiotto, L. Xian, D. A. Rhodes, C. Tan, M. Claassen, D. M. Kennes, Y. Bai, B. Kim *et al.*, Correlated electronic phases in twisted bilayer transition metal dichalcogenides, *Nat. Mater.* **19**, 861 (2020).
- [20] A. Ghiotto, E.-M. Shih, G. S. S. G. Pereira, D. A. Rhodes, B. Kim, J. Zang, A. J. Millis, K. Watanabe, T. Taniguchi, J. C. Hone *et al.*, Quantum criticality in twisted transition metal dichalcogenides, *Nature (London)* **597**, 345 (2021).
- [21] Z. Zhang, Y. Wang, K. Watanabe, T. Taniguchi, K. Ueno, E. Tutuc, and B. J. LeRoy, Flat bands in twisted bilayer transition metal dichalcogenides, *Nat. Phys.* **16**, 1093 (2020).
- [22] S. Shabani, D. Halbertal, W. Wu, M. Chen, S. Liu, J. Hone, W. Yao, D. N. Basov, X. Zhu, and A. N. Pasupathy, Deep moiré potentials in twisted transition metal dichalcogenide bilayers, *Nat. Phys.* **17**, 720 (2021).
- [23] A. Weston, Y. Zou, V. Enaldiev, A. Summerfield, N. Clark, V. Zólyomi, A. Graham, C. Yelgel, S. Magorrian, M. Zhou *et al.*, Atomic reconstruction in twisted bilayers of transition metal dichalcogenides, *Nat. Nanotechnol.* **15**, 592 (2020).
- [24] X. Liu, Z. Hao, E. Khalaf, J. Y. Lee, Y. Ronen, H. Yoo, D. Haei Najafabadi, K. Watanabe, T. Taniguchi, A. Vishwanath, and P. Kim, Tunable spin-polarized correlated states in twisted double bilayer graphene, *Nature (London)* **583**, 221 (2020).
- [25] C. Shen, Y. Chu, Q. Wu, N. Li, S. Wang, Y. Zhao, J. Tang, J. Liu, J. Tian, K. Watanabe *et al.*, Correlated states in twisted double bilayer graphene, *Nat. Phys.* **16**, 520 (2020).
- [26] G. Chen, L. Jiang, S. Wu, B. Lyu, H. Li, B. L. Chittari, K. Watanabe, T. Taniguchi, Z. Shi, J. Jung *et al.*, Evidence of a gate-tunable Mott insulator in a trilayer graphene moiré superlattice, *Nat. Phys.* **15**, 237 (2019).
- [27] G. Chen, A. L. Sharpe, P. Gallagher, I. T. Rosen, E. J. Fox, L. Jiang, B. Lyu, H. Li, K. Watanabe, T. Taniguchi *et al.*, Signatures of tunable superconductivity in a trilayer graphene moiré superlattice, *Nature (London)* **572**, 215 (2019).
- [28] G. Chen, A. L. Sharpe, E. J. Fox, Y.-H. Zhang, S. Wang, L. Jiang, B. Lyu, H. Li, K. Watanabe, T. Taniguchi *et al.*, Tunable correlated Chern insulator and ferromagnetism in a moiré superlattice, *Nature (London)* **579**, 56 (2020).
- [29] Y. Cao, D. Rodan-Legrain, O. Rubies-Bigorda, J. M. Park, K. Watanabe, T. Taniguchi, and P. Jarillo-Herrero, Tunable correlated states and spin-polarized phases in twisted bilayer-bilayer graphene, *Nature (London)* **583**, 215 (2020).
- [30] M. He, Y. Li, J. Cai, Y. Liu, K. Watanabe, T. Taniguchi, X. Xu, and M. Yankowitz, Symmetry breaking in twisted double bilayer graphene, *Nat. Phys.* **17**, 26 (2021).
- [31] J. M. Park, Y. Cao, K. Watanabe, T. Taniguchi, and P. Jarillo-Herrero, Tunable strongly coupled superconductivity in magic-angle twisted trilayer graphene, *Nature (London)* **590**, 249 (2021).
- [32] Z. Zhu, S. Carr, D. Massatt, M. Luskin, and E. Kaxiras, Twisted trilayer graphene: A precisely tunable platform for correlated electrons, *Phys. Rev. Lett.* **125**, 116404 (2020).
- [33] H. Polshyn, M. Yankowitz, S. Chen, Y. Zhang, K. Watanabe, T. Taniguchi, C. R. Dean, and A. F. Young, Large linear-in-temperature resistivity in twisted bilayer graphene, *Nat. Phys.* **15**, 1011 (2019).
- [34] Y. Cao, D. Chowdhury, D. Rodan-Legrain, O. Rubies-Bigorda, K. Watanabe, T. Taniguchi, T. Senthil, and P. Jarillo-Herrero, Strange metal in magic-angle graphene with near planckian dissipation, *Phys. Rev. Lett.* **124**, 076801 (2020).
- [35] R. Lyu, Z. Tuchfeld, N. Verma, H. Tian, K. Watanabe, T. Taniguchi, C. N. Lau, M. Randeria, and M. Bockrath, Strange metal behavior of the Hall angle in twisted bilayer graphene, *Phys. Rev. B* **103**, 245424 (2021).
- [36] M. Serlin, C. L. Tschirhart, H. Polshyn, Y. Zhang, J. Zhu, K. Watanabe, T. Taniguchi, L. Balents, and A. F. Young, Intrinsic quantized anomalous Hall effect in a moiré heterostructure, *Science* **367**, 900 (2020).
- [37] C.-C. Tseng, X. Ma, Z. Liu, K. Watanabe, T. Taniguchi, J.-H. Chu, and M. Yankowitz, Anomalous Hall effect at half filling in twisted bilayer graphene, *Nat. Phys.* **18**, 1038 (2022).

- [38] T. Neupert, L. Santos, C. Chamon, and C. Mudry, Fractional quantum Hall states at zero magnetic field, *Phys. Rev. Lett.* **106**, 236804 (2011).
- [39] D. N. Sheng, Z.-C. Gu, K. Sun, and L. Sheng, Fractional quantum Hall effect in the absence of Landau levels, *Nat. Commun.* **2**, 389 EP (2011).
- [40] N. Regnault and B. A. Bernevig, Fractional Chern insulator, *Phys. Rev. X* **1**, 021014 (2011).
- [41] J. Cai, E. Anderson, C. Wang, X. Zhang, X. Liu, W. Holtzmann, Y. Zhang, F. Fan, T. Taniguchi, K. Watanabe *et al.*, Signatures of fractional quantum anomalous Hall states in twisted MoTe₂, *Nature (London)* **622**, 63 (2023).
- [42] Y. Zeng, Z. Xia, K. Kang, J. Zhu, P. Knüppel, C. Vaswani, K. Watanabe, T. Taniguchi, K. F. Mak, and J. Shan, Integer and fractional Chern insulators in twisted bilayer MoTe₂, [arXiv:2305.00973](https://arxiv.org/abs/2305.00973).
- [43] H. Park, J. Cai, E. Anderson, Y. Zhang, J. Zhu, X. Liu, C. Wang, W. Holtzmann, C. Hu, Z. Liu *et al.*, Observation of fractionally quantized anomalous Hall effect, *Nature (London)* **622**, 74 (2023).
- [44] F. Xu, Z. Sun, T. Jia, C. Liu, C. Xu, C. Li, Y. Gu, K. Watanabe, T. Taniguchi, B. Tong, J. Jia, Z. Shi, S. Jiang, Y. Zhang, X. Liu, and T. Li, Observation of integer and fractional quantum anomalous Hall effects in twisted bilayer MoTe₂, *Phys. Rev. X* **13**, 031037 (2023).
- [45] R. Bistritzer and A. H. MacDonald, Moiré bands in twisted double-layer graphene, *Proc. Natl. Acad. Sci. USA* **108**, 12233 (2011).
- [46] J. M. B. Lopes dos Santos, N. M. R. Peres, and A. H. Castro Neto, Graphene bilayer with a twist: Electronic structure, *Phys. Rev. Lett.* **99**, 256802 (2007).
- [47] G. Tarnopolsky, A. J. Kruchkov, and A. Vishwanath, Origin of magic angles in twisted bilayer graphene, *Phys. Rev. Lett.* **122**, 106405 (2019).
- [48] G. Tarnopolsky, A. J. Kruchkov, and A. Vishwanath, Origin of magic angles in twisted bilayer graphene, *Phys. Rev. Lett.* **122**, 106405 (2019).
- [49] F. Wu, T. Lovorn, E. Tutuc, and A. H. MacDonald, Hubbard model physics in transition metal dichalcogenide moiré bands, *Phys. Rev. Lett.* **121**, 026402 (2018).
- [50] J. Kang and O. Vafek, Symmetry, maximally localized Wannier states, and a low-energy model for twisted bilayer graphene narrow bands, *Phys. Rev. X* **8**, 031088 (2018).
- [51] N. Bultinck, E. Khalaf, S. Liu, S. Chatterjee, A. Vishwanath, and M. P. Zaletel, Ground state and hidden symmetry of magic-angle graphene at even integer filling, *Phys. Rev. X* **10**, 031034 (2020).
- [52] B. A. Bernevig, Z.-D. Song, N. Regnault, and B. Lian, Twisted bilayer graphene. III. Interacting Hamiltonian and exact symmetries, *Phys. Rev. B* **103**, 205413 (2021).
- [53] B. Estienne, N. Regnault, and V. Crépel, Ideal Chern bands as Landau levels in curved space, *Phys. Rev. Research* **5**, L032048 (2023).
- [54] P. J. Ledwith, G. Tarnopolsky, E. Khalaf, and A. Vishwanath, Fractional Chern insulator states in twisted bilayer graphene: An analytical approach, *Phys. Rev. Research* **2**, 023237 (2020).
- [55] F. Wu and S. Das Sarma, Collective excitations of quantum anomalous Hall ferromagnets in twisted bilayer graphene, *Phys. Rev. Lett.* **124**, 046403 (2020).
- [56] N. Bultinck, S. Chatterjee, and M. P. Zaletel, Mechanism for anomalous Hall ferromagnetism in twisted bilayer graphene, *Phys. Rev. Lett.* **124**, 166601 (2020).
- [57] J. Liu and X. Dai, Theories for the correlated insulating states and quantum anomalous Hall effect phenomena in twisted bilayer graphene, *Phys. Rev. B* **103**, 035427 (2021).
- [58] Y.-H. Zhang, D. Mao, and T. Senthil, Twisted bilayer graphene aligned with hexagonal boron nitride: Anomalous Hall effect and a lattice model, *Phys. Rev. Research* **1**, 033126 (2019).
- [59] J. Liu, J. Liu, and X. Dai, Pseudo Landau level representation of twisted bilayer graphene: Band topology and implications on the correlated insulating phase, *Phys. Rev. B* **99**, 155415 (2019).
- [60] F. Wu, T. Lovorn, E. Tutuc, I. Martin, and A. H. MacDonald, Topological insulators in twisted transition metal dichalcogenide homobilayers, *Phys. Rev. Lett.* **122**, 086402 (2019).
- [61] H. Pan, F. Wu, and S. Das Sarma, Band topology, Hubbard model, Heisenberg model, and Dzyaloshinskii-Moriya interaction in twisted bilayer WSe₂, *Phys. Rev. Research* **2**, 033087 (2020).
- [62] J. Zang, J. Wang, J. Cano, and A. J. Millis, Hartree-fock study of the moiré Hubbard model for twisted bilayer transition metal dichalcogenides, *Phys. Rev. B* **104**, 075150 (2021).
- [63] Y.-M. Wu, Z. Wu, and H. Yao, Pair-density-wave and chiral superconductivity in twisted bilayer transition metal dichalcogenides, *Phys. Rev. Lett.* **130**, 126001 (2023).
- [64] D. Mao, K. Zhang, and E.-A. Kim, Fractionalization in fractional correlated insulating states at $n \pm 1/3$ filled twisted bilayer graphene, *Phys. Rev. Lett.* **131**, 106801 (2023).
- [65] C. L. Kane and E. J. Mele, Quantum spin Hall effect in graphene, *Phys. Rev. Lett.* **95**, 226801 (2005).
- [66] C. L. Kane and E. J. Mele, Z₂ topological order and the quantum spin Hall effect, *Phys. Rev. Lett.* **95**, 146802 (2005).
- [67] B. A. Bernevig and S.-C. Zhang, Quantum spin Hall effect, *Phys. Rev. Lett.* **96**, 106802 (2006).
- [68] B. A. Bernevig, T. L. Hughes, and S.-C. Zhang, Quantum spin Hall effect and topological phase transition in HgTe quantum wells, *Science* **314**, 1757 (2006).
- [69] D. N. Sheng, Z. Y. Weng, L. Sheng, and F. D. M. Haldane, Quantum spin-Hall effect and topologically invariant Chern numbers, *Phys. Rev. Lett.* **97**, 036808 (2006).
- [70] W. Li, D. N. Sheng, C. S. Ting, and Y. Chen, Fractional quantum spin Hall effect in flat-band checkerboard lattice model, *Phys. Rev. B* **90**, 081102(R) (2014).
- [71] M. O. Goerbig, From fractional Chern insulators to a fractional quantum spin Hall effect, *Eur. Phys. J. B* **85**, 15 (2012).
- [72] T. Li, S. Jiang, B. Shen, Y. Zhang, L. Li, Z. Tao, T. Devakul, K. Watanabe, T. Taniguchi, L. Fu *et al.*, Quantum anomalous Hall effect from intertwined moiré bands, *Nature (London)* **600**, 641 (2021).
- [73] W. Zhao, K. Kang, L. Li, C. Tschirhart, E. Redekop, K. Watanabe, T. Taniguchi, A. Young, J. Shan, and K. F. Mak, Realization of the Haldane Chern insulator in a moiré lattice, [arXiv:2207.02312](https://arxiv.org/abs/2207.02312).
- [74] B. A. Foutty, C. R. Kometter, T. Devakul, A. P. Reddy, K. Watanabe, T. Taniguchi, L. Fu, and B. E. Feldman, Mapping twist-tuned multi-band topology in bilayer WSe₂, [arXiv:2304.09808](https://arxiv.org/abs/2304.09808).

- [75] M. Levin and A. Stern, Fractional topological insulators, *Phys. Rev. Lett.* **103**, 196803 (2009).
- [76] T. Neupert, L. Santos, S. Ryu, C. Chamon, and C. Mudry, Fractional topological liquids with time-reversal symmetry and their lattice realization, *Phys. Rev. B* **84**, 165107 (2011).
- [77] L. Santos, T. Neupert, S. Ryu, C. Chamon, and C. Mudry, Time-reversal symmetric hierarchy of fractional incompressible liquids, *Phys. Rev. B* **84**, 165138 (2011).
- [78] P. Bampoulis, C. Castenmiller, D. J. Klaassen, J. van Mil, Y. Liu, C.-C. Liu, Y. Yao, M. Ezawa, A. N. Rudenko, and H. J. W. Zandvliet, Quantum spin Hall states and topological phase transition in germanene, *Phys. Rev. Lett.* **130**, 196401 (2023).
- [79] Z. Meng, L. Wang, W. Han, F. Liu, K. Wen, C. Gao, P. Wang, C. Chin, and J. Zhang, Atomic Bose–Einstein condensate in twisted-bilayer optical lattices, *Nature (London)* **615**, 231 (2023).
- [80] Here we approximately assume that δ is the same for both layers.
- [81] D. Xiao, G.-B. Liu, W. Feng, X. Xu, and W. Yao, Coupled spin and valley physics in monolayers of MoS₂ and other group-VI dichalcogenides, *Phys. Rev. Lett.* **108**, 196802 (2012).
- [82] N. J. Roome and J. D. Carey, Beyond graphene: Stable elemental monolayers of silicene and germanene, *ACS Appl. Mater. Interfaces* **6**, 7743 (2014).
- [83] M. Z. Hasan and C. L. Kane, Colloquium: Topological insulators, *Rev. Mod. Phys.* **82**, 3045 (2010).
- [84] P. Castro, D. Shaffer, Y.-M. Wu, and L. H. Santos, Emergence of the Chern supermetal and pair-density wave through higher-order van Hove singularities in the Haldane-Hubbard model, *Phys. Rev. Lett.* **131**, 026601 (2023).
- [85] Y.-M. Wu, R. Thomale, and S. Raghu, Sublattice interference promotes pair density wave order in kagome metals, *Phys. Rev. B* **108**, L081117 (2023).
- [86] M. L. Kiesel and R. Thomale, Sublattice interference in the kagome Hubbard model, *Phys. Rev. B* **86**, 121105(R) (2012).
- [87] The sublattice weight for the n th band is defined as $u_{A/B}^{(n)} = \sum_I |u_{I,n}^{(A/B)}|^2$ where $u_{I,n}^{(A/B)}$ is the eigenstate for the n th band projected to A/B sublattice and I is the shorthand of the indices other than sublattice.
- [88] S. Kharchev and A. Zabrodin, Theta vocabulary I, *J. Geom. Phys.* **94**, 19 (2015).
- [89] F. D. M. Haldane, A modular-invariant modified Weierstrass sigma-function as a building block for lowest-Landau-level wavefunctions on the torus, *J. Math. Phys.* **59**, 071901 (2018).
- [90] One caveat here is that $\chi_{st,k}$ is a two-component wavefunction, with each component from distinct layers shifted by \mathbf{q}_1 from each other. Bloch's theorem for χ_{st} thus implies $\chi_{st,k}(\mathbf{r} + \mathbf{a}) = e^{ik \cdot \mathbf{a}} \text{diag}(1, e^{i\mathbf{q}_1 \cdot \mathbf{a}}) \chi_{st,k}(\mathbf{r})$.
- [91] F. D. M. Haldane and E. H. Rezayi, Periodic Laughlin-Jastrow wave functions for the fractional quantized Hall effect, *Phys. Rev. B* **31**, 2529 (1985).
- [92] J. Wang, J. Cano, A. J. Millis, Z. Liu, and B. Yang, Exact Landau level description of geometry and interaction in a flatband, *Phys. Rev. Lett.* **127**, 246403 (2021).
- [93] P. J. Ledwith, A. Vishwanath, and D. E. Parker, Vortexability: A unifying criterion for ideal fractional Chern insulators, [arXiv:2209.15023](https://arxiv.org/abs/2209.15023).
- [94] S. M. Girvin, A. H. MacDonald, and P. M. Platzman, Magneto-roton theory of collective excitations in the fractional quantum Hall effect, *Phys. Rev. B* **33**, 2481 (1986).
- [95] S. A. Parameswaran, R. Roy, and S. L. Sondhi, Fractional Chern insulators and the W_∞ algebra, *Phys. Rev. B* **85**, 241308(R) (2012).
- [96] R. Roy, Band geometry of fractional topological insulators, *Phys. Rev. B* **90**, 165139 (2014).
- [97] M. Claassen, C. H. Lee, R. Thomale, X.-L. Qi, and T. P. Devereaux, Position-momentum duality and fractional quantum Hall effect in Chern insulators, *Phys. Rev. Lett.* **114**, 236802 (2015).
- [98] J. Zak, Magnetic translation group, *Phys. Rev.* **134**, A1602 (1964).
- [99] M. König, S. Wiedmann, C. Brune, A. Roth, H. Buhmann, L. W. Molenkamp, X.-L. Qi, and S.-C. Zhang, Quantum spin Hall insulator state in HgTe quantum wells, *Science* **318**, 766 (2007).
- [100] D. L. Maslov and M. Stone, Landauer conductance of Luttinger liquids with leads, *Phys. Rev. B* **52**, R5539(R) (1995).
- [101] R. De-Picciotto, M. Reznikov, M. Heiblum, V. Umansky, G. Bunin, and D. Mahalu, Direct observation of a fractional charge, *Phys. B: Condens. Matter* **249-251**, 395 (1998).
- [102] L. Saminadayar, D. C. Glatli, Y. Jin, and B. Etienne, Observation of the $e/3$ fractionally charged Laughlin quasiparticle, *Phys. Rev. Lett.* **79**, 2526 (1997).
- [103] S. A. Trugman and S. Kivelson, Exact results for the fractional quantum Hall effect with general interactions, *Phys. Rev. B* **31**, 5280 (1985).
- [104] P. Mai, J. Zhao, B. E. Feldman, and P. W. Phillips, $1/4$ is the new $1/2$ when topology is intertwined with Mottness, *Nat Commun* **14**, 5999 (2023).
- [105] K. Kang, B. Shen, Y. Qiu, K. Watanabe, T. Taniguchi, J. Shan, and K. F. Mak, Observation of the fractional quantum spin Hall effect in moiré MoTe₂, [arXiv:2402.03294](https://arxiv.org/abs/2402.03294).